Interplay of magnetic order, pairing, and phase separation in a one-dimensional spin-fermion model

Wenjian Hu, Richard T. Scalettar, and Rajiv R. P. Singh
Department of Physics, University of California, Davis, California 95616, USA
(Received 19 June 2015; revised manuscript received 14 August 2015; published 16 September 2015)

We consider a lattice model of itinerant electrons coupled to an array of localized classical Heisenberg spins. The nature of the ground-state-ordered magnetic phases that result from the indirect spin-spin coupling mediated by the electrons is determined as a function of density and the spin-fermion coupling J. At a fixed chemical potential, spiral phases exist only up to values of J which are less than roughly half the electronic bandwidth. At a fixed electron density and near half filling, the system phase-separates into a half-filled antiferromagnetic phase and a spiral phase. The ferromagnetic phases are shown to be fully polarized, while the spiral phases have equal admixture of up and down spins. Phase separation survives in the presence of weak pairing field Δ but disappears when Δ exceeds a critical value Δ_c. If pairing fields are large enough, an additional spiral state arises at strong coupling J. The relevance of this study, especially the phase separation, to artificially engineered systems of adjacent itinerant electrons and localized spins is discussed. In particular, we propose a method which might allow for the braiding of Majorana fermions by changing the density and moving their location as they are pulled along by a phase separation boundary.

DOI: 10.1103/PhysRevB.92.115133 PACS number(s): 75.10.Pq, 71.10.Hf, 71.10.Pm

I. INTRODUCTION

Many-body effects in solids are commonly explored either by Hamiltonians which include explicit electron-electron interactions, e.g., the Hubbard or periodic Anderson models, or else by Hamiltonians containing interactions of free electrons with other (quantum spin or phonon) degrees of freedom, e.g., the Kondo or Holstein models, respectively. The distinction between these two descriptions is not completely sharp; the Kondo model is a large-U limit of the periodic Anderson model, for example. Even more generally, the introduction of auxiliary fields allows the mapping of Hamiltonians with direct electron-electron interactions to free fermions coupled to a "Hubbard-Stratonovich" field. In all these cases, the quantum spin, phonon, or Hubbard-Stratonovich variables depend on both space and imaginary time.

Suppressing the imaginary-time dependence represents an approximation to including the full effect of quantum fluctuations. Nevertheless, many of the interesting effects of electronic interactions can still be studied in this regime. This approximation has been motivated, for example, in cases where large ("classical") core spins are coupled to an itinerant electron band, a situation which occurs in the double perovskite Sr_2FeMoO_6 where the $3d^5$ configuration of Fe^{3+} forms a spin-5/2 with which the Mo electron interacts [1–3]. Similarly, applications of classical spin-fermion models to a broad class of materials including nickelates [4,5], cuprate superconductors [6], and iron superconductors [7–9] have been reported, with the elucidation of subtle many-body effects including magnetic and charge domain formation, and site-selective Mott transitions. In these materials, the coupling of an itinerant electron band to classical degrees of freedom is argued to capture the quantum mechanics of fast electronic motion in contact with the slower degrees of freedom, much in the spirit of the Born-Oppenheimer approximation or the Car-Parrinello method [10].

In a technically similar spirit of treating interactions by a simplified time-independent variable that leaves the electronic problem quadratic, proximity-induced superconductivity can be described by a pairing field bilinear in fermion operators [11]. The combined effects of frozen spin and pairing configurations lead to many interesting features including topological superconductivity and Majorana states [12,13].

The realizations of spin-fermion models described above have largely concerned tight-binding Hamiltonians where the electrons move on a lattice. Very recently, the approach was also applied to a gas of fermions moving in the continuum in one dimension, but coupled to a regular array of classical spins [14]. The itinerant electrons mediate a Ruderman-Kittel-Kasuya-Yoshida (RKKY) [15–17] interaction. The goal of the work was to determine the ground state phase diagram in the plane of the exchange coupling between the classical and electron spins and the electron density, and explore the possibility of spiral spin states driving one-dimensional superconductors into topological phases [18–21].

In this paper we study the lattice version of this problem (see also [25]). We show that, similarly to the continuum case, ferromagnetism (F) occurs at low filling and is replaced by a spiral configuration of classical spins, which minimizes the energy only when the exchange constant J is smaller than roughly half the bandwidth W. The spiral phase gives way to commensurate antiferromagnetic (AF) order as J increases. One central observation of our work is that near half filling and at a fixed electron density, the system phase-separates into a half-filled AF phase and a spiral phase of reduced (less than half filling) or enhanced (greater than half filling) density at weak coupling $J \lesssim W/2 = 2t$. We show that this spiral-AF phase separation initially survives in the presence of a weak pairing field Δ, but for larger Δ the transition becomes continuous. We observe that the effect of Δ is richer at strong coupling J. For Δ small the transition from AF to F is direct, without an intervening spiral phase, and exhibits phase separation. With increasing Δ, a spiral phase emerges. The spiral to AF transition is initially discontinuous, but becomes continuous for larger values of Δ. We discuss the implication of these results for an artificially engineered system of adjacent itinerant electrons and localized spins.

II. MODEL AND METHODS

We first consider a lattice of one-dimensional itinerant electrons coupled to classical Heisenberg spins $\vec{S}_l$ in the grand-canonical ensemble (GCE),

$$H = -t\sum_{l\sigma}(c^\dagger_{l+1\sigma}c_{l\sigma} + c^\dagger_{l\sigma}c_{l+1\sigma}) - \mu\sum_{l\sigma} n_{l\sigma} + J\sum_l \vec{s}_l\cdot\vec{S}_l. \quad (1)$$

Here the fermionic spin components are $s_{lx} = c^\dagger_{l\uparrow}c_{l\downarrow} + c^\dagger_{l\downarrow}c_{l\uparrow}$; $s_{ly} = -ic^\dagger_{l\uparrow}c_{l\downarrow} + ic^\dagger_{l\downarrow}c_{l\uparrow}$; and $s_{lz} = c^\dagger_{l\uparrow}c_{l\uparrow} - c^\dagger_{l\downarrow}c_{l\downarrow}$.

A single spin in a conduction electron sea induces a magnetic polarization which can then couple to other spins, so that the itinerant electrons mediate an RKKY interaction. At $T = 0$ this interaction falls off as $1/r^d$ in d dimensions, and oscillates in phase with the Fermi wave vector k_F. A classical Ising model in $d = 1$ with (unfrustrated) power law interactions $J(r) \sim 1/r^p$ has no long-range order at finite T if $p > 2$, but orders, with mean-field exponents, for $1 < p < 3/2$. Order at finite T with continuously varying exponent occurs in between these cases $3/2 < p < 2$. For $p < 1$ ordering occurs at all T. 1D classical Heisenberg spins with power law interactions also have long-range order at finite temperature for $1 < p < 2$ but no transition for $p \geqslant 2$ [22], which suggests that, in principle, the $1/r$ RKKY long-range interaction could result in spin ordering at $T > 0$ in one dimension. However, for finite temperatures the power law is multiplied by a decaying exponential $e^{-r/\xi(T)}$, with correlation length $\xi(T)$ diverging at $T = 0$. Thus one expects only (possibly rapid) crossovers to quasiordered phases at $T \neq 0$.

Since H is quadratic in the fermion creation and destruction operators, it may be solved for an arbitrary Heisenberg spin configuration $\{\vec{S}_l\}$ by diagonalizing a matrix of dimension $2L$, where L is the number of sites in the chain. The factor of 2 arises from the mixing of the fermionic spin components through their coupling to $\{\vec{S}_l\}$. The competition between the Fermi vector k_F, which depends on doping, and the AF exchange leads to a spiral phase [23,24], where the classical Heisenberg spins form a spiral magnetic structure. We do not consider arbitrary Heisenberg spin configurations $\{\vec{S}_l\}$ and instead make an ansatz of a spiral configuration [25,26]. The most general such form is $\vec{S}_l = \hat{x}\cos(q_1 l)\cos(q_2 l + \phi) + \hat{y}\cos(q_1 l)\sin(q_2 l + \phi) + \hat{z}\sin(q_1 l)$, which, in zero external field, should further simplify to a planar form $\vec{S}_l = \hat{x}\cos(ql) + \hat{y}\sin(ql)$. Here allowed q values with periodic boundary conditions are $q = n\frac{2\pi}{L}$, $n = 0,1,2,3,\ldots,(L-1)$. Because of the rotational symmetry of the fermionic part of the Hamiltonian, the properties are equivalent with other choices for the spin plane. Likewise, symmetry dictates that q and $(2\pi - q)$ yield the same physics.

While the full $2L$ dimensional matrix must be considered to solve Eq. (1) in the case of arbitrary $\{S_l\}$ through a full matrix diagonalization, with this planar, spiral ansatz, the Hamiltonian can be solved in momentum space: $c^\dagger_{l\sigma} = (1/\sqrt{N})\sum_k e^{-ikl}c^\dagger_{k\sigma}$. For a specific q, spin $\uparrow$ fermions of momentum $k - q$ are mixed only with spin $\downarrow$ fermions of momentum k and the Hamiltonian H becomes a sum of independent 2×2 blocks:

$$H_q = \sum_k\{-2t[\cos(k-q)c^\dagger_{k-q\uparrow}c_{k-q\uparrow} + \cos(k)c^\dagger_{k\downarrow}c_{k\downarrow}] + J(c^\dagger_{k-q\uparrow}c_{k\downarrow} + c^\dagger_{k\downarrow}c_{k-q\uparrow}) - \mu(c^\dagger_{k-q\uparrow}c_{k-q\uparrow} + c^\dagger_{k\downarrow}c_{k\downarrow})\}. \quad (2)$$

This Hamiltonian produces two energy bands,

$$E_\pm = -t[\cos k + \cos(k-q)] - \mu \pm \sqrt{\{t[\cos k - \cos(k-q)]\}^2 + J^2}. \quad (3)$$

We select $t = 1$ to set our energy scale.

As reviewed in the introduction, it is of interest to extend the model in Eq. (1) to include Δ in the Hamiltonian:

$$H_\Delta = -t\sum_{l\sigma}(c^\dagger_{l+1\sigma}c_{l\sigma} + c^\dagger_{l\sigma}c_{l+1\sigma}) - \mu\sum_{l\sigma} n_{l\sigma} + J\sum_l \vec{s}_l\cdot\vec{S}_l + \sum_l(\Delta c^\dagger_{l\uparrow}c^\dagger_{l\downarrow} + \text{H.c.}). \quad (4)$$

Part of the results in this paper will be to determine the effect of Δ on the phase diagram, specifically, phase separation. To find the ground state energy, the Hamiltonian can again be transformed to momentum space. The combination of the spin up/down mixing due to J and the pairing yields a 4×4 structure,

$$H_\Delta = \frac{1}{2}\sum_k \vec{v_k}^\dagger M_k \vec{v_k} + \frac{1}{2}\sum_k[\epsilon_{-(k-q)} + \epsilon_{-k}], \quad (5)$$

where $\epsilon_{k-q} = \epsilon_{-(k-q)} = -2t\cos(k-q) - \mu$, $\epsilon_k = \epsilon_{-k} = -2t\cos(k) - \mu$, $\vec{v_k}^\dagger = [c^\dagger_{k-q,\uparrow} \quad c^\dagger_{k,\downarrow} \quad c_{-(k-q),\downarrow} \quad c_{-k,\uparrow}]$, and

$$M_k = \begin{bmatrix} \epsilon_{k-q} & J & \Delta & 0 \\ J & \epsilon_k & 0 & \Delta \\ \Delta & 0 & -\epsilon_{-(k-q)} & -J \\ 0 & \Delta & -J & -\epsilon_{-k} \end{bmatrix}. \quad (6)$$

M_k has four eigenvalues, λ_1, λ_2, λ_3, λ_4 ($\lambda_1 > \lambda_2 > 0 > \lambda_3 > \lambda_4$) and the corresponding normalized eigenvectors $\vec{v}_1$, $\vec{v}_2$, $\vec{v}_3$, $\vec{v}_4$. We define a new set of operators:

$$\begin{bmatrix} \gamma_{k,1} \\ \gamma_{k,2} \\ \gamma^\dagger_{k,3} \\ \gamma^\dagger_{k,4} \end{bmatrix} = S_k^T \begin{bmatrix} c_{k-q,\uparrow} \\ c_{k,\downarrow} \\ c^\dagger_{-(k-q),\downarrow} \\ c^\dagger_{-k,\uparrow} \end{bmatrix}, \quad (7)$$

where the matrix $S_k = [\vec{v}_1, \vec{v}_2, \vec{v}_3, \vec{v}_4]$. In terms of these new canonical operators,

$$H_\Delta = \frac{1}{2}\sum_k[\lambda_1\gamma^\dagger_{k,1}\gamma_{k,1} + \lambda_2\gamma^\dagger_{k,2}\gamma_{k,2} - \lambda_3\gamma^\dagger_{k,3}\gamma_{k,3} - \lambda_4\gamma^\dagger_{k,4}\gamma_{k,4} + \lambda_3 + \lambda_4 + \epsilon_k + \epsilon_{k-q}]. \quad (8)$$

Since the ground state has no excited quasiparticles, the ground state energy is

$$E_0 = \frac{1}{2}\sum_k [\lambda_3(k) + \lambda_4(k) + \epsilon_k + \epsilon_{k-q}]$$
$$= \frac{1}{2}\sum_k [\lambda_3(k) + \lambda_4(k)] - L\mu. \quad (9)$$

III. MAGNETIC PHASE DIAGRAM

We first consider $\Delta = 0$. For each J we determine the optimal ordering wave vector q_* by minimizing the ground state energy, obtained by summing all eigenenergies of Eq. (2) up to the desired chemical potential μ. Typical results are shown in Fig. 1. We see that F order is preferred at low density, and gives way first to spiral and then AF order as μ increases at fixed $J = 1$. At $J = 2.5$, there is a direct phase transition from F to AF. The Hamiltonian Eq. (1) is particle-hole symmetric, so the optimal q is the same for $-\mu$ and $+\mu$.

Performing the calculation in Fig. 1 for different J generates the ground state phase diagram of Fig. 2. The topology is qualitatively similar to the continuum reported in Ref. [14]. The $J = 0$ corners of the spiral phase are at $\mu = \pm 2t$ where one enters/leaves the band. The precise value J_c above which the spiral phase vanishes must be determined numerically. However, we expect J_c to the same order as t, as is the case in the continuum model [14] where $J_c \sim \sqrt{\mu/m}$, where μ is the chemical potential and m is the effective mass, since in the lattice model $\mu \sim t$ and $m \sim 1/t$. In particular, for all chemical potentials, spiral order gives way to AF order as J increases. A difference is the almost linear AF phase boundaries we find here. This near linearity is a consequence of the dispersion relation in the AF phase on a lattice, $E_{\mathrm{AF}\pm} = \pm\sqrt{J^2 + 4t^2\cos^2 k}$, which gives a gap $\Delta_{AF} = 2J$. When the chemical potential μ is in the gap $-J < \mu < J$, the density is pinned at half filling, where the AF phase dominates.

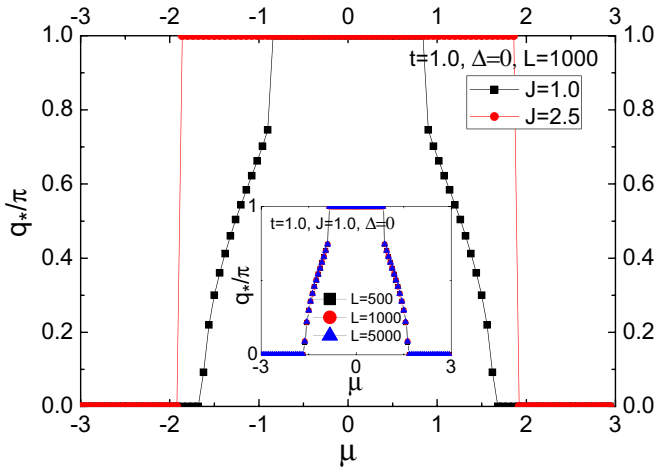

FIG. 1. (Color online) Classical spin wave vector q_* which minimizes the ground state energy, as a function of chemical potential μ for fixed $J = 1.0$ and $J = 2.5$. Inset: Red circles denote results with lattice size $L = 1000$ sites. Data for $L = 500$ (black squares) and $L = 5000$ (blue triangles) indicate finite-size effects are small.

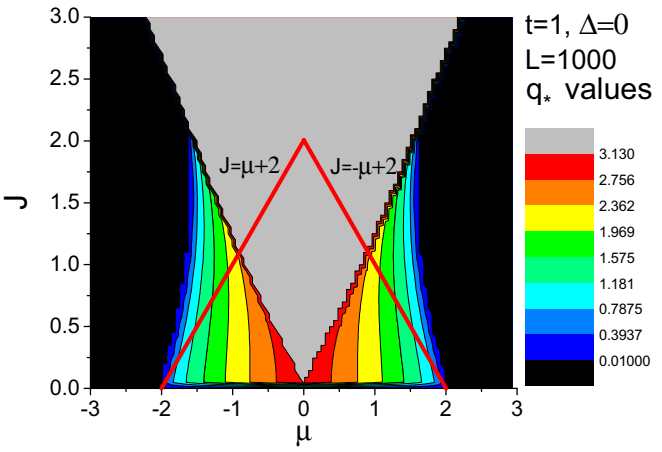

FIG. 2. (Color online) Phase diagram in the chemical potential (μ), exchange constant (J) plane. At low and high densities (the Hamiltonian is particle-hole symmetric) ferromagnetic order $q_* = 0$ minimizes the energy. For $J \lesssim W/2 = 2t$, F order gives way first to spiral (incommensurate q_*) and then AF ($q_* = \pi$) order. The red lines mark the boundary between full and partial polarization in a F state. See text.

Thus, in the absence of phase separation, we expect linear AF phase boundaries. As described further below, however, this argument must be refined because of the occurrence of phase separation. Another distinction from the continuum model is the particle-hole symmetry of Eq. (1). In the continuum system, ρ can extend to arbitrarily large values, as opposed to the maximal density $\rho = 2$ fermions per site in the lattice case.

One can ask whether the F order is fully or partially polarized. By "fully polarized" we mean that either the majority spin density equals the total density ρ and the minority spin density vanishes (below half filling), or the majority spin density is saturated at unity and the minority spin density is $\rho - 1$ (above half filling). That is, the system is as polarized as possible, consistent with its overall particle density. Because our spiral state is in the xy plane, we consider $N_{x\sigma} = \sum_l \langle c^\dagger_{l,x\sigma} c_{l,x\sigma}\rangle$, where $c_{l,x\sigma} = (c_{l\uparrow} + \sigma c_{l\downarrow})/\sqrt{2}$ in terms of the operators $c_{l\uparrow}$ and $c_{l\downarrow}$ which create fermions with spin up/down in the z direction at site l. At $q_* = 0$ the eigenspectrum is $E_{\mathrm{F}\pm} = -2t\cos k - \mu \pm J$. For small J, the upper band E_+ will begin to be occupied for relatively low chemical potential (density). As J increases, full polarization persists to larger chemical potential (density). The red lines in Fig. 2 give the values of J above which partial polarization occurs. These lie entirely in the spiral portion of the phase diagram, so that we conclude only fully polarized F phases occur.

Further details on the magnetic phases can be obtained by separately computing the densities of the two spin species as functions of chemical potential. This is shown in Fig. 3. The vertical lines are the magnetic boundaries, which are perfectly aligned with abrupt changes in $N_{x\sigma}$. The fully polarized nature of the F phase is emphasized by the fact that the density of one species is zero below entrance into the spiral phase, at which point the two species become equally populated.

Figure 4 shows the density as a function of chemical potential for a cut across the phase boundary at $J = 1$. There

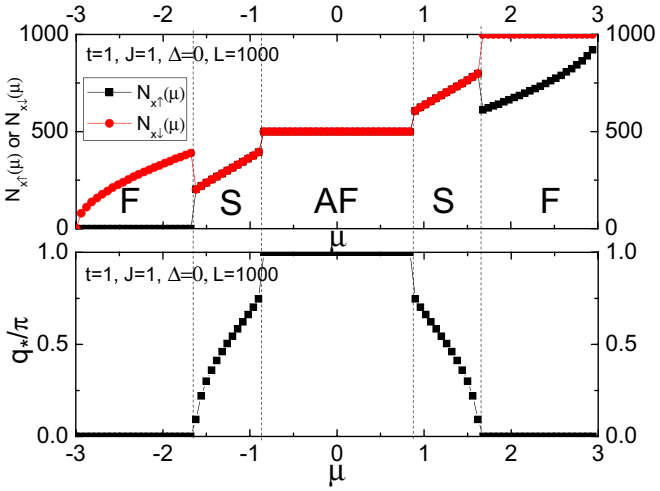

FIG. 3. (Color online) Top: Populations of the individual species with spin in the $\pm\hat{x}$ directions, as functions of chemical potential. The F phase at low (and high) density is fully polarized, while the spiral and AF phases have balanced populations. Bottom: The corresponding ground state (F, S, or AF). Discontinuities in $N_{x\sigma}$ occur precisely at the magnetic phase boundaries.

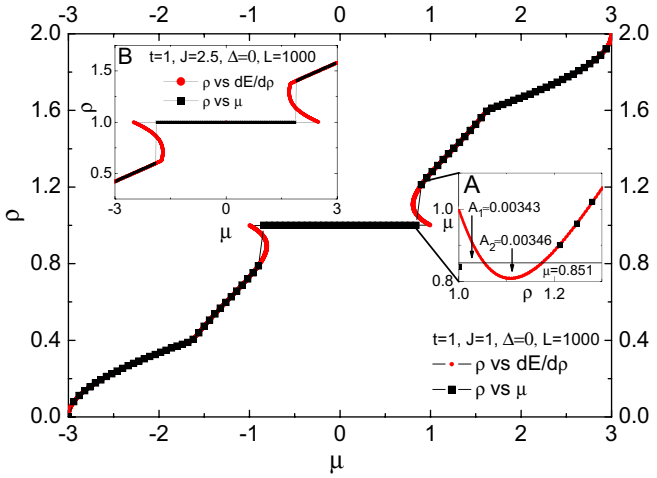

FIG. 5. (Color online) Density is shown as a function of chemical potential in the graph. Black squares denote ρ vs μ in the GCE. Red circles denote ρ vs $\mu = dE_0/d\rho$ in the CE. Inset A: Enlarged μ vs ρ graph. The two areas $A_1 \approx A_2$ satisfy the Maxwell construction. Here the critical μ is 0.851. Inset B: ρ vs μ in GCE and ρ vs $dE/d\rho$ in CE at $J = 2.5$, which shows a direct phase transition from F to AF.

is a kink in $\rho(\mu)$ at $\mu \approx -1.63$ where the compressibility $\kappa = d\rho/d\mu$ jumps upon entering the spiral phase from the ferromagnet. ρ is discontinuous at the entry to the AF phase from spiral order. The plateau at $\rho = 1$ extends over a range of μ roughly given by the AF gap $\Delta_{\rm AF} = 2J$ at $q_* = \pi$. (See above). For the case $J = 2.5$, density ρ is also discontinuous. The plateau range at $\rho = 1$ is somewhat less than $2J$, which is shown in inset B of Fig. 4. Entrance into the AF phase is from the F phase rather than the spiral phase.

The discontinuity in q_* at the spiral-AF boundary and the F-AF boundary seen in Fig. 1 indicates the presence of spiral-AF phase separation and F-AF phase separation,

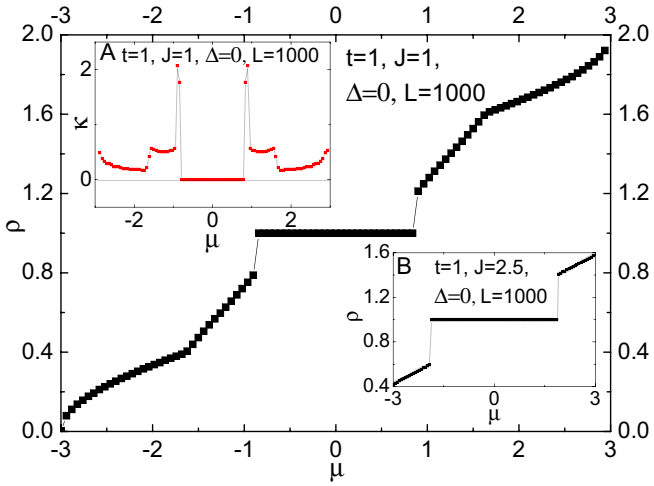

FIG. 4. (Color online) Density as a function of chemical potential at $J = 1$. The F-spiral phase boundary is signaled by a jump in the compressibility $\kappa = d\rho/d\mu$. The density jumps abruptly at the spiral-AF boundary. Inset A: Compressibility κ vs μ. Inset B: Density as a function of μ at $J = 2.5$.

which is consistent with the discontinuity in ρ in Fig. 4. This presence of this first-order phase transition agrees with the continuum case [14]. The case of spiral-AF phase separation is further discussed below. At $J = 1$ there is a thermodynamically unstable range of densities $0.823 \lesssim \rho < 1$ where separate AF and spiral domains coexist. This can be further probed by working in the canonical ensemble (CE) and computing the chemical potential via a finite difference $\mu = E_0(N + 1) - E_0(N)$. Here E_0 denotes the ground state energy per site. As N increases past a critical value, μ begins to decrease so that $\kappa = d\rho/d\mu < 0$. Phrased alternatively, the ground state energy is concave down, $d^2E_0/d\rho^2 < 0$. This indicates the boundary of the region of phase separation around half filling. For a lattice with those values of ρ, the energy can be lowered by phase-separating into distinct spiral and AF regions. We have verified that the Maxwell equal-area construction is satisfied, which is as expected at the spiral-AF first-order phase transition.

The main panel of Fig. 5 gives ρ as a function of μ for both the CE and GCE at $J = 1$. The negative curvature of $E_0(\rho)$ in the CE is reflected in the bending back of the CE curve for $\rho(\mu)$. This signature of phase separation at the spiral to AF boundary also occurs at the F to AF boundary, as shown for $J = 2.5$ in inset B of Fig. 5.

To probe the details of coexistence further, we verified that the fractions f $(1 - f)$ of the chain in the spiral (AF) phases obey

$$\rho = \rho_S f + \rho_{\rm AF}(1 - f), \tag{10}$$

where ρ is the overall mixture density, $\rho_{\rm AF}$ equals 1.0, and $\rho_S(J)$ is the spiral state density in the mixture. For example, at $J = 1$, $\rho_S = 0.823$. This relation is also obeyed for phase separation at the F-AF boundary, with ρ_S replaced by ρ_F. For $J = 2.5$ we find $\rho_F = 0.598$.

The energy bands, $E(k)$, and the momentum distribution function of the original fermion operators, $n(k)$, in the spiral

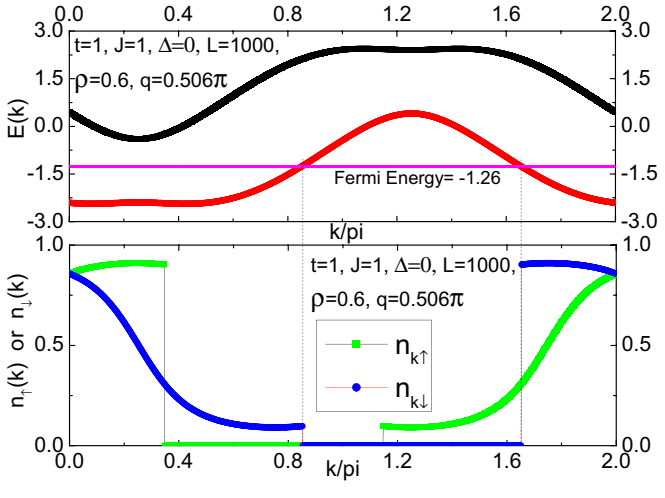

FIG. 6. (Color online) Top: The mixing of k with $k-q$, for $q = 0.506\pi$, gives rise to a pair of overlapping energy bands. Bottom: Occupation numbers in the k space. The jumps of $n_\uparrow(k)$ or $n_\downarrow(k)$ curves show Fermi wave vectors k_F.

phase are shown in Fig. 6. An important feature to note is that only one band crosses the Fermi energy. We have further checked that the entanglement entropy of the system corresponds to that of spinless fermions. Because the new electronic eigenoperators are superpositions of two different k states in the original basis, $n(k)$ shows discontinuity at four wave vectors.

Turning on Δ and minimizing the ground state energy E_0 [see Eq. (9)] results in the optimal ordering wave vector q_* in Fig. 7 and Fig. 8. J mixes fermion modes of momenta k and $k-q$ for a classical spin configuration of wave vector q, and at the same time Δ mixes k,σ and $-k,-\sigma$. Together, the result is the four hybridized bands of Eqs. (6) and (7). The ground

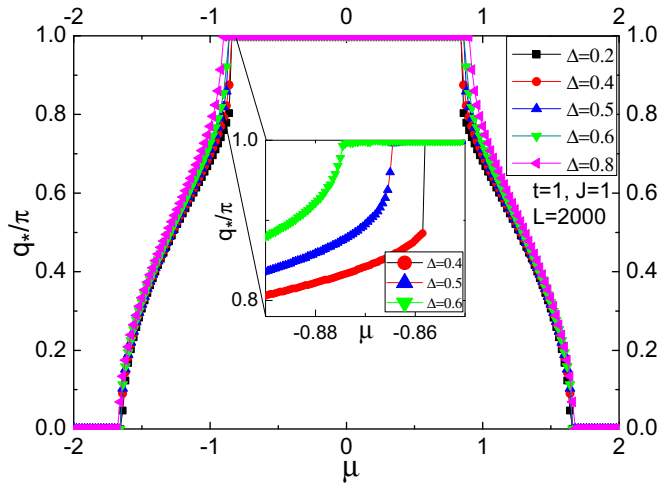

FIG. 7. (Color online) Optimal wave vector q_* which minimizes the ground state energy E_0, as a function of chemical potential μ for fixed $J = 1.0$ but different Δ values. Finite-size effects are verified to be small. Inset: Enlarged q_*/π vs μ graph. It has an abrupt jump at $\Delta = 0.4$ but grows continuously at $\Delta = 0.6$. $\Delta = 0.5$ is around the critical value Δ_c.

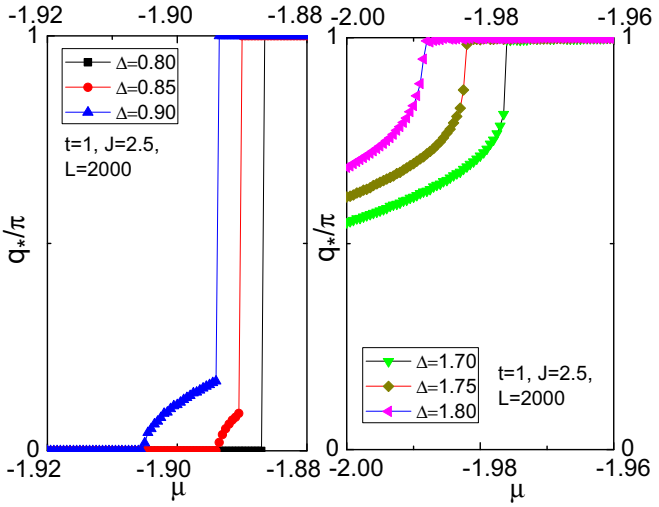

FIG. 8. (Color online) Optimal wave vector q_* as a function of chemical potential μ for fixed $J = 2.5$ but different Δ values. There are two critical values Δ_c for $J = 2.5$. Left: Wave vector q_* vs μ for $\mu \approx \Delta_c^-$. This lower Δ_c^- distinguishes F-AF phase separation and spiral-AF phase separation. Right: Wave vector q_* vs μ for $\mu \approx \Delta_c^+$. The upper Δ_c^+ distinguishes spiral-AF phase separation and no phase separation.

state is determined by minimizing the sum of the energies of levels $\lambda_3(k)$ and $\lambda_4(k)$ which develop from $-\epsilon_{-(k-q)}$ and $-\epsilon_{-k}$, respectively. In Fig. 7, at $J = 1.0$, the former favors a spiral phase $q_* \neq \pi$, while the latter is minimized by an AF $q_* = \pi$. We find that increasing Δ enhances the effect of $\lambda_4(k)$, that is, makes its AF minima more pronounced than that of the spiral minima in $\lambda_3(k)$. This is reflected in the growth of the size of the AF region with Δ. Changing Δ from 0.2 to 0.8, the spiral wave vector q_* increases, and results in the disappearance of spiral-AF phase separation at the critical value Δ_c. We saw in

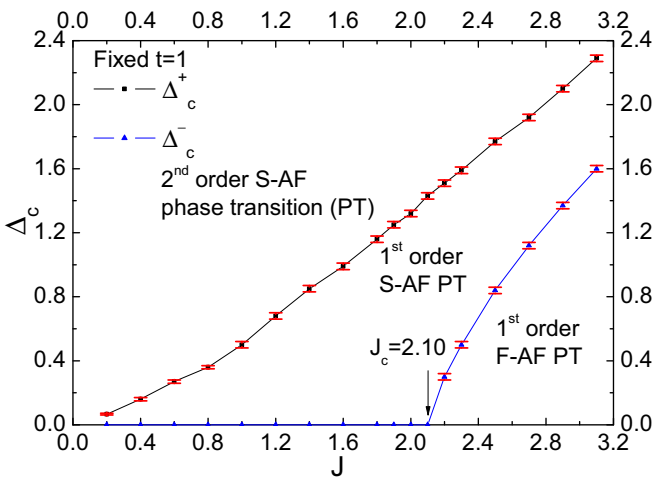

FIG. 9. (Color online) Critical value Δ_c vs exchange constant J. There are two critical values, upper Δ_c^+ and lower Δ_c^-, for fixed J. Below the critical value $J_c = 2.10 \pm 0.02$, only Δ_c^+ is nonzero. There are three regions distinguished by second-order spiral-AF phase transition (PT), first-order spiral-AF PT, and first-order F-AF PT.

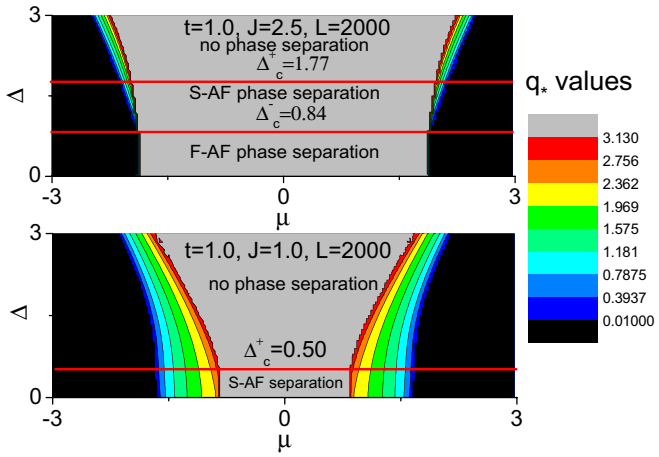

FIG. 10. (Color online) Top: Phase diagram in the chemical potential (μ), pairing field (Δ) plane, with fixed exchange constants ($J = 2.5$). The upper red line corresponds to upper Δ_c^+. The lower red line corresponds to lower Δ_c^-. Bottom: Phase diagram in μ, Δ plane, with fixed $J = 1.0$. The red line corresponds to Δ_c^+. Δ_c^- is zero at $J = 1.0$.

Fig. 2 that for $J \gtrsim 2t$ the spiral region terminates and only a direct F to AF transition occurs. An interesting effect of the pairing term Δ is that, if it takes a sufficiently large value, it stabilizes the spiral phase at $J \gtrsim 2t$. Figure 8 (left) shows results for q_* at $J = 2.5$. When $\Delta = 0.80$, there is still a direct F ($q_* = 0$) to AF ($q_* = \pi$) jump. However at $\Delta = 0.85$ a spiral phase with intermediate q_* is evident. We define a lower Δ_c^- to be the critical Δ above which the spiral is stabilized by pairing. The jump in q_* at the S to AF transition which emerges steadily shrinks as Δ grows further. In fact, ultimately the jump goes to zero at an upper Δ_c^+. At this point the spiral to AF transition no longer exhibits phase separation. This behavior is shown in Fig. 8 (right).

The shrinking of the jump in q_* at the spiral to AF transition also occurs for $J \lesssim 2t$ where the spiral phase is stable even at $\Delta = 0$ (that is, when $\Delta_c^- = 0$). Figure 9 shows the critical values Δ_c^- and Δ_c^+ as functions of J, and three regions with their different types of phase transitions.

The phase diagram of Eq. (4), which models a spin-fermion system in contact with an s-wave superconductor, depends on the parameters μ, J, and Δ. Figure 2 is the cut of the resulting 3D phase diagram at $\Delta = 0$. We now explore several cuts in the μ,Δ plane at fixed J. The resulting phase boundaries are shown for $J = 1.0$ and $J = 2.5$ in Fig. 10. (The Hamiltonian H_Δ is still particle-hole symmetric, so the diagrams are symmetric about $\mu = 0$.) In the bottom graph ($J = 1.0$), for which the spiral phase is stable even in the absence of pairing, the effect of increasing Δ is to expand the stability of the AF, and shrink the range of chemical potential for which the spiral exists. The horizontal line shows the location of Δ_c^+ where the spiral to AF transition becomes continuous and no longer exhibits phase separation. The stabilization of the AF appears to onset at Δ_c^+. In the top graph ($J = 2.5$), for which the spiral is not stable in the absence of pairing, there is a more rich behavior. Although the F and AF phases dominate, a range of spiral phase arises above Δ_c^- (lower horizontal line) and leads to spiral-AF phase separation near half filling. When $\Delta > \Delta_c^+$ (upper horizontal line) phase separation disappears and the transition from spiral phase to AF phase becomes continuous.

IV. DISCUSSION AND CONCLUSIONS

In this paper, we have computed the ground state magnetic phase diagram of one-dimensional fermions on a lattice coupled to classical Heisenberg spins. Ferromagnetism occurs at low and high densities, and occurs only in full polarization. Spiral phases give way to commensurate order as the spin-fermion coupling increases. At weak coupling J the system is thermodynamically unstable at the spiral-AF phase boundary, with separate AF and spiral domains present in a range of densities near half filling, while at strong coupling J, the system is thermodynamically unstable at the F-AF phase boundary. The Maxwell construction is verified in the phase separation. With the introduction of Δ, at weak coupling J, spiral-AF phase separation survives at weak Δ but totally disappears when Δ exceeds the critical value. At strong coupling J, the system evolves from F-AF phase separation through spiral-AF phase separation to no phase separation with the increase of Δ. We should note that spiral phases may be less favorable if the overall system is higher dimensional.

A potentially exciting application of itinerant electrons interacting with localized spins is in the context of artificially engineered systems with magnetic atoms on the surface of a metal or a superconductor. Indeed, the search for Majorana fermions in such hybrid magnetic-superconducting systems is a hot topic [12,27,28] of current research. Vazifeh *et al.* [20,21,25] have shown that, within a BCS treatment, when fermions are coupled to a spiral spin configuration topological phases are robust and hence Majorana end states should be expected [13]. The existence of phase separation between spiral and antiferromagnetic (AF) states implies that, with pairing, such Majorana fermions might move away from chain ends to the interface between spiral and AF phases. This means that by changing the electronic density, one may be able to move the location of the Majorana particles. This could be helpful in the braiding of these excitations in a network of chains. This issue deserves further consideration.

ACKNOWLEDGMENTS

This work was supported in part by National Science Foundation Grant No. DMR-1306048 and by the Office of the President of the University of California.

[1] O. Erten, O. N. Meetei, A. Mukherjee, M. Randeria, N. Trivedi, and P. Woodward, Phys. Rev. Lett. **107**, 257201 (2011).

[2] P. Sanyal and P. Majumdar, Phys. Rev. B **80**, 054411 (2009).

[3] O. N. Meetei, O. Erten, A. Mukherjee, M. Randeria, N. Trivedi, and P. Woodward, Phys. Rev. B **87**, 165104 (2013).

[4] S. Johnston, A. Mukherjee, I. Elfimov, M. Berciu, and G. A. Sawatzky, Phys. Rev. Lett. **112**, 106404 (2014).
[5] H. Park, A. J. Millis, and C. A. Marianetti, Phys. Rev. Lett. **109**, 156402 (2012).
[6] C. Buhler, S. Yunoki, and A. Moreo, Phys. Rev. Lett. **84**, 2690 (2000).
[7] W.-G. Yin, C-C. Lee, and W. Ku, Phys. Rev. Lett. **105**, 107004 (2010).
[8] W. Lv, F. Krüger, and P. Phillips, Phys. Rev. B **82**, 045125 (2010).
[9] S. Liang, A. Moreo, and E. Dagotto, Phys. Rev. Lett. **111**, 047004 (2013).
[10] R. Car and M. Parrinello, Phys. Rev. Lett. **55**, 2471 (1985).
[11] A. Y. Kitaev, Phys. Usp. **44**, 131 (2001).
[12] J. Alicea, Rep. Prog. Phys. **75**, 076501 (2012).
[13] J. D. Sau, S. Tewari, and S. Das Sarma, Phys. Rev. B **85**, 064512 (2012).
[14] M. Schecter, M. S. Rudner, and K. Flensberg, Phys. Rev. Lett. **114**, 247205 (2015).
[15] M. A. Ruderman and C. Kittel, Phys. Rev. **96**, 99 (1954).
[16] T. Kasuya, Prog. Theor. Phys. **16**, 45 (1956).
[17] K. Yosida, Phys. Rev. **106**, 893 (1957).
[18] F. Pientka, L. I. Glazman, and F. von Oppen, Phys. Rev. B **88**, 155420 (2013).
[19] F. Pientka, L. I. Glazman, and F. von Oppen, Phys. Rev. B **89**, 180505(R) (2014).
[20] B. Braunecker and P. Simon, Phys. Rev. Lett. **111**, 147202 (2013).
[21] J. Klinovaja, P. Stano, A. Yazdani, and D. Loss, Phys. Rev. Lett. **111**, 186805 (2013).
[22] A. Cavallo, F. Cosenza, and L. De Cesare, Phys. Rev. B **66**, 174439 (2002).
[23] B. Braunecker, P. Simon, and D. Loss, Phys. Rev. Lett. **102**, 116403 (2009).
[24] B. Braunecker, P. Simon, and D. Loss, Phys. Rev. B **80**, 165119 (2009).
[25] M. M. Vazifeh and M. Franz, Phys. Rev. Lett. **111**, 206802 (2013).
[26] I. Reis, D. J. J. Marchand, and M. Franz, Phys. Rev. B **90**, 085124 (2014).
[27] S. Nadj-Perge, I. K. Drozdov, B. A. Bernevig, and Ali Yazdani, Phys. Rev. B **88**, 020407(R) (2013).
[28] S. Nadj-Perge, I. K. Drozdov, J. Li, H. Chen, S. Jeon, J. Seo, A. H. MacDonald, B. A. Bernevig, and A. Yazdani, Science **346**, 602 (2014).